ACS OMEGA

Open Access



http://pubs.acs.org/journal/acsodf

Article

# Intrinsically Antibacterial Carbon Nanoparticles Optimally Entangle into Polymeric Films to Produce Composite Packaging

Neha Yadav, Debmalya Roy, and Santosh K. Misra*

Cite This: *ACS Omega* 2024, 9, 45104−45116

Read Online

ACCESS | Metrics & More | Article Recommendations | Supporting Information

**ABSTRACT:** The quality of food, pharmaceutical, or sustainability products is generally maintained through optimal storage conditions or the use of packaging films. Herein, an intrinsically antibacterial and improvised polylactic acid-based film (*hpp*-PLA-film) has been produced by introducing a microwave-assisted synthesis process of carbon nanoparticles produced from hemp fibers (*hf*-CNPs). These high-performance packaging (*hpp*-PLA) films were produced with different percentages of loaded *hf*-CNPs, i.e., 0.05 and 0.5% (w/w), called *hpp*-PLA-0.05-film and *hpp*-PLA-0.5-film, respectively. The chemical entangling of *hf*-CNPs in PLA films was probed by various physicochemical, thermal, and mechanical characterization methods. The antibacterial properties of *hpp*-PLA-films could inhibit bacterial growth and outperform kanamycin, at least for longer time periods. Overall, it could be established that the produced *hpp*-PLA-0.05-film not only was better in mechanical, antibacterial, dissolution, and physical impact sustainability but also had biodegradation properties and may be a better alternative for regular PLA-based packaging composites in the near future.

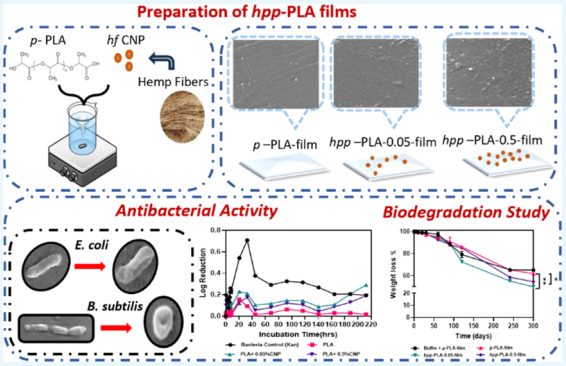


## 1. INTRODUCTION

Packaging is to help keep the objects inside fresh, sterile, clean, and safe for the intended shelf life through physical protection during transport, handling, and storage. It also protects from humidity, light, heat, and other external factors, maintaining information transmission about the product and its safety and providing added convenience in distribution, stacking, and ease of disposal.[1] Petrochemical polymers, as materials to package food, are often used due to their excellent mechanical properties and low cost. However, these materials cause substantial environmental difficulties, as they are difficult to biodegrade, resulting in long-term waste and contamination. In response to these environmental concerns, there has been growing interest in producing packaging materials made of biodegradable polymers and biodegradable polymer composites.[2−4] Most of the biodegradable polymers are derived from natural sources,[3] have the advantage of decomposition through natural processes including soil moisture, microorganisms, oxygen, and are mineralized into carbon dioxide, nitrogen, and water. The natural degradation is enabled by the nature of these polymers, making them a more ecologically benign option compared with their petrochemical counterparts. Despite their environmental benefits, natural biodegradable polymers tend to have inferior mechanical , barrier properties and lower thermal stability than other petrochemical-based alternatives.[5−10] These restrictions can impair their effectiveness in packaging applications, where durability and protection against external forces are critical. Thus, a new material with good mechanical properties and biodegradability could be a better option. Polylactic acid (*p*-PLA) has emerged as a viable answer to these difficulties. It is a biodegradable plastic that offers a balance between environmental sustainability and practical performance that is comparable to petroleum-derived plastics in terms of cost, processing ease, and market availability. Moreover, *p*-PLA is an aliphatic polyester noted for its environment-friendly manufacturing along with better biocompatibility and degradation properties.[5−8] The *p*-PLA is produced from the condensation of lactic acid via ring-opening polymerization.[11−14]

Biodegradable packaging made from polymers, which possess antibacterial properties too, either inherently or through the integration of antibacterial components into polymers, can provide enhanced benefits.[10,15,16] Such antibacterial, polymeric packaging materials can be classified based on the polymeric matrix and antibacterial agents used in the preparation (Table S1). Earlier, different types of antibacterial components like essential oils (e.g., cinnamon essential oil), plant extracts (e.g., lemon extract), bacteriocins (e.g., nisin), enzymes (such as lysozyme), chitosan, organic acids (such as lauric acid), metal nanocomposites (such as silver nano-

Received: June 19, 2024
Revised: September 11, 2024
Accepted: September 16, 2024
Published: October 29, 2024

particles), and chelating agents (such as EDTA) have been used successfully.[13,14,17] Antibacterial agents have distinct inhibitory activity against certain microorganisms, and determining the level that must be incorporated to effectively inhibit the bacteria is paramount.[18,19] Further, depending on the mechanism of action of the antibacterial agents, packaging systems can be classified into three types—release, absorption, and immobilization.[19] The third type of antibacterial packaging is preferred due to the long-term bacterial inhibition possibility. Thus, to make an optimum packaging material, a biodegradable polymer can be incorporated with natural antibacterials with the immobilization method. The process of producing natural antibacterial components generally determines biocompatibility and degradability, but durability and heat resistance remain limiting factors.[20−25] To circumvent these limitations, either antibacterial agents are incorporated into nanomaterial systems or nanomaterials with inherent antibacterial properties can be synthesized. Carbon nanomaterials (CNMs) could be such nanomaterials that can work as performance enhancers for thermal, chemical, optical, and mechanical properties of polymers,[26−28] whereas intrinsic antibacterial properties might be inculcated due to the source material used in the process of synthesizing these CNPs. By keeping these learnings in mind, to reinforce the concept of environment-friendly packaging with enhanced performance and intrinsic antibacterial properties, *hf*-CNPs have been synthesized from natural hemp fibers.[29−32]

Hemp fibers are known to have antibacterial properties due to phenolic acid and aldehyde components (vanillin, syringaldehyde, vanillic acid, syringic acid, etc.),[33] which would remain intact if CNPs are produced from them by the microwave method. Herein, we used the microwave method to produce *hf*-CNPs, which were further optimally incorporated in PLA films to generate high-performance polymeric PLA films, named *hpp*-PLA-films. These films were characterized for chemical, mechanical, thermal, morphological, surface, and biological properties and compared with parent films of PLA, named *p*-PLA. To show the efficiency of these *hpp*-PLA-films, a model scenario of using a packaging film for essentials to drop in flood-like situations was considered. A pocket water filtration cartridge unit was used as a model essential for packaging with *hpp*-PLA-films and demonstrating the efficiency in simulated operational conditions.[34]

## 2. MATERIALS AND METHODS

**2.1. Materials.** The hemp fibers were supplied by Vruksha Composites (India). Polylactic acid (Mw ∼ 60,000) was procured from Sigma-Aldrich (India). The chemicals used were analytical grade and sourced locally. The chemicals utilized during nanoparticle synthesis include sodium hydroxide (NaOH), hydrogen peroxide ($H_2O_2$), sulfuric acid ($H_2SO_4$), thiourea ($NH_2CSNH_2$), and ethanol ($C_2H_5OH$). Chemical chloroform ($CHCl_3$) was used to dissolve *p*-PLA during film formation. The Luria−Bertani broth and kanamycin for antibacterial studies were procured from HiMedia (India) and Sigma-Aldrich (India), respectively. The spin coater accessory was purchased from M/S Vision Scientific (India).

**2.2. Synthesis and Characterization of Intrinsically Antibacterial Carbon Nanoparticles Produced from Hemp Fibers (*hf*-CNPs).** Carbon nanoparticles are known to be synthesized by microwave synthesis followed by centrifugation from different carbon sources (e.g., sucrose).[35,36] We utilized the same process in a microwave synthesizer to effectively control the input parameters. The carbon source utilized was microcellulose extracted through acid digestion from hemp fibers.

*2.2.1. Extraction of Microcellulose.* The acquired hemp fibers were washed with Milli-Q water to remove residual dust and dried for 12 h in a hot air oven at 80 °C to eradicate excess moisture. The fibers were ground to a powder form before being added to 20 mL of 5 M NaOH at 80 °C with vigorous stirring for 4 h. After NaOH treatment, the fibers were washed thoroughly with Milli-Q water to remove the remaining alkali. The bleaching of fibers was carried out in 3 mg/mL of 147 mM $H_2O_2$, pH 10.5, for 1 h at 55 °C followed by washing. Then, 35% $H_2SO_4$ was added to bleached fibers and treated for 4 h at room temperature with high-speed stirring. Finally, the fibers were washed until all acid residues were removed. The obtained microcellulose (MC) residue was dried to produce a powder form by the process of lyophilization.

*2.2.2. Microwave Synthesis of Carbon Nanoparticles.* The generated MC was then treated with 12% (w/w) thiourea at room temperature for 1 h at 130 °C in a microwave synthesizer. The synthesized nanoparticle suspension was sonicated for 30 min before being centrifuged at 3000 rpm for 10 min. The centrifuge was further sonicated to increase the homogeneity of the nanoparticles. The suspension was further centrifuged at different centrifugation speeds (5000, 10,000, and 15,000 rpm). The pellet was resuspended in ethanol and sonicated multiple times along with centrifugation at 10,000 rpm for 10 min. The nanoparticles produced from hemp fibers (*hf*-CNPs) were stored at 4 °C. The *hf*-CNP suspensions collected after 5000, 10,000, and 15,000 rpm were used for particle size determination by using dynamic light scattering.

**2.3. Preparation and Characterization of Optimally Entangling of *hf*-CNPs in Polylactic Acid Solution to Produce High-Performance Packaging (*hpp*-PLA) Films.**

*2.3.1. Preparation of hpp-PLA- Films.* The procured PLA (MW 60,000, Sigma-Aldrich, 10% w/v) was dissolved in chloroform (10 mL) and poured into a glass Petri dish for preparation of *p*-PLA-films. In another aliquot of 10 mL of chloroform solution of PLA, 5 mL of an ethanol suspension of *hf*-CNP was added drop by drop with continuous stirring to form a homogeneous solution. The *hf*-CNP-PLA suspension was then poured into a glass Petri dish and allowed to dry at room temperature for the next 2 days. For safe handling, chloroform was always used in a chemical fume hood with appropriate protective gear to avoid contact with skin, eyes, and clothing. In the event of spills or leaks, chloroform was absorbed with an inert material and disposed of as hazardous waste in a sealed container, ensuring it did not enter drains or the environment.

*2.3.2. Characterization of hpp-PLA-Films.* A rectangular-shaped sample of the *hpp*-PLA-film (thickness 0.1 ± 0.02 mm, base width 14 ± 0.2 mm, and base length 17 ± 0.2 mm) was prepared. The tensile strength of these films was measured in an Instron dynamometer (model 1195) at a crosshead speed of 5 mm/min with an initial length of 20 mm. The thermogravimetric measurements were performed in a TA-TGA Q500 thermal analyzer. The experiments were performed under a nitrogen atmosphere in dynamic mode. Each crucible was heated from 25 to 800 °C at 10 °C/min. The primary degradation temperatures ($T_0$) were established at 8% weight loss, whereas the maximum degradation rate ($T_{max}$) was


https://doi.org/10.1021/acsomega.4c05732
ACS Omega 2024, 9, 45104−45116

analyzed from the first derivative of the TGA curves. The optical transmittance spectra were measured in a UV/Visible spectrophotometer. The spectra were quantified in the range of 200−800 nm. The wettability was measured by using an optical tensiometer (DataPhysics OCA). The surface topography and roughness of the *hpp*-PLA -film were measured through atomic force microscopy (A.P.E. Research A100). The scanning area was 10 $\mu$m × 10 $\mu$m, and the vertical range was 6 $\mu$m. The specimens were prepared to meet the specific imaging criteria of AFM, affixed to the sample platform using double-sided adhesive tape, and examined using non-contact scanning mode. A sharpened cantilever was used to obtain images, which were then processed into 3D images. In order to maintain consistency, images were taken from the center region of each surface. The roughness values of three distinct zones of each sample were calculated by analyzing them offline using Gwyddion software. The measured roughness characteristics consisted of the average roughness ($S_a$), root-mean-square roughness ($S_q$), and the slope for each point of the area, except the edge points ($S_{dq}$). The *hpp*-PLA-film samples were further characterized by FTIR spectroscopy (Bruker Tensor) at 23 °C. The spectra in the range of 4000−400 $cm^{-1}$ with automatic signal gain were amassed at 1 $cm^{-1}$ spectral resolution.

*2.3.3. Dissolution Studies of hpp-PLA-Films in Aqueous and Buffered Medium.* 100 mg of the *p*-PLA-film and *hpp*-PLA-films were submerged in Milli-Q water with stirring at 100 rpm for 7 days. The samples were collected at 1, 2, 3, 4, and 8 h time intervals for short-term dissolution studies. In long-term dissolution studies, the samples were collected from the first day to the seventh day at intervals of 24 h. Absorbance was recorded from 200 to 800 nm against Milli-Q water.[37,38] A 1× PBS solution was prepared with pH (8.5) where 100 mg of *p*-PLA-films and *hpp*-PLA-films were submerged in PBS with stirring at 100 rpm for 7 days. The samples were collected at 1, 2, 3, 4, and 8 h time intervals for short-term dissolution studies. In long-term dissolution studies, the samples were collected from the first day to the seventh day at intervals of 24 h. Absorbance was recorded from 200 to 800 nm against 1× PBS buffer.

*2.3.4. Antibacterial Properties of hpp-PLA Films.* *E. coli* and *B. subtilis* were used to assess the antibacterial activity of these *hpp*-PLA films. Bacteria were grown aerobically in LB media at 37 °C with shaking (120 rpm) to an optical density of 0.2 at 600 nm. The *p*-PLA and *hpp*-PLA films (200 mg/mL) were added to the bacterial culture. The bacterial culture without any addition was taken as a negative control, whereas kanamycin was used as a positive control. The bacterial culture with *p*-PLA and *hpp*-PLA-films was aerobically incubated at 37 °C with continuous shaking (120 rpm). The samples were collected from the incubated bacterial culture at 0, 0.5, 1, 1.5, 2, 2.5, 3, 3.5, 4, 5, 6, 7, 8, 10, 12, 24, 48, 72, 96, 120, 144, and 168 h after incubation.[39] The optical density was recorded at 600 nm to compute bacterial growth. The changed morphology of bacteria after coming in contact with the *hpp*-PLAfilm was imaged by SEM (Zeiss EVO 18) after 8 h of incubation. For sample imaging, the *p*-PLA-film and *hpp*-PLA-films with growing bacteria were washed twice with phosphate-buffered saline (PBS). The films were further immersed in a 3.5% formaldehyde solution for 15 min to affix the bacterial cells. Then, film samples were dipped serially in 30, 50, 70, 90, and 100% ethanol, respectively to eliminate water from the samples. A Quorum sputter coater was used to coat a 15 nm gold thin layer to evade the charging effect.

*2.3.5. Wrapping Feasibility and Drop Test.* A model object of a pocket water filtration cartridge unit with air-droppable characteristics was used to study the wrapping feasibility of produced films and the effect of *hf*-CNP incorporation in *p*-PLA-films. Objects of higher weight (500 g) and dimension (0.5 L capacity) were wrapped with the *p*-PLA film and *hpp*-PLA-films and used for the drop test. The wrapped objects are oriented vertically, facing upward, which is the most challenging position for object testing, and dropped from 80 feet height on the cement floor. The impact on objects was analyzed through photographic images captured before and after the drop test.

*2.3.6. Biodegradation Study.* Two simulated conditions were used to study the biodegradability of the produced films. Triplicate samples of *p*-PLA and *hpp*-PLA-films, each weighing 50 mg, were buried at a depth of 4−6 cm in perforated plastic boxes containing microbially active soil with a humus content of 2% and a water content of 22−24%. The samples were then incubated at 37 °C under aerobic conditions and recovered after 1, 2, 3, 6, 8, 10, 15, and 30 days of disintegration.[40,41] Following each extraction, all samples were washed, dried, and weighed to qualitatively assess the degree of physical degradation in the compost as a function of time. This system was developed to imitate the natural composting conditions that plastics normally meet, including crucial elements such as temperature, moisture, and aeration, assuring an accurate reproduction of real-world composting situations. Alternatively, *p*-PLA and *hpp*-PLA-films (25 mg) were kept in glass vials and immersed in the enzyme lipase solution or TRIS buffer, as required. Following that, samples in the vials were stirred at 200 rpm and 37 °C. Furthermore, the evaluation of the degradation process included the measurement of the principal degradation product, lactic acid, in addition to tracking weight loss. The monomer reacts with iron(III) chloride hexahydrate to form a complex that exhibits a peak absorption at 390 nm in the UV−vis spectrum. A solution of the reagent (3 mg/mL) was made, and 2 mL of this solution was combined with 50 $\mu$L of the degradation medium to create the complex. The initial measurement was conducted by combining 2 mL of the reagent with 50 $\mu$L of buffer. The device scanned between 230 and 800 nm with a resolution of 1 nm. The *p*-PLA and *hpp*-PLA-films were removed from the vial at predetermined intervals, washed with water, dried, weighed, and then reimmersed in the same solution. This enzyme-based degradation investigation was conducted continuously for 300 days at 37 °C with consistent stirring to achieve uniform conditions. The same set of samples were utilized throughout the experiment, as shown in Figure 6, to maintain homogeneity. The samples were incubated under controlled conditions at 37 °C with regular monitoring to prevent any degradation beyond the experimental settings. In addition to the measurement of weight loss, enzymatic degradation was determined through the main degradation product, lactic acid. Lactic acid is known to form a complex with iron(III) chloride hexahydrate with an adsorption peak at 390 nm. The complex was formed when 3 mL of the reagent solution (1 mg/mL) was mixed with 75 $\mu$L of the degradation medium. The control was measured using 3 mL of the reagent and 75 $\mu$L of buffer. The absorbance spectra were collected in a quartz cuvette of 1 cm path length and 1 nm resolution in a wavelength range of 230−800 nm.[40,41]


https://doi.org/10.1021/acsomega.4c05732
ACS Omega 2024, 9, 45104−45116

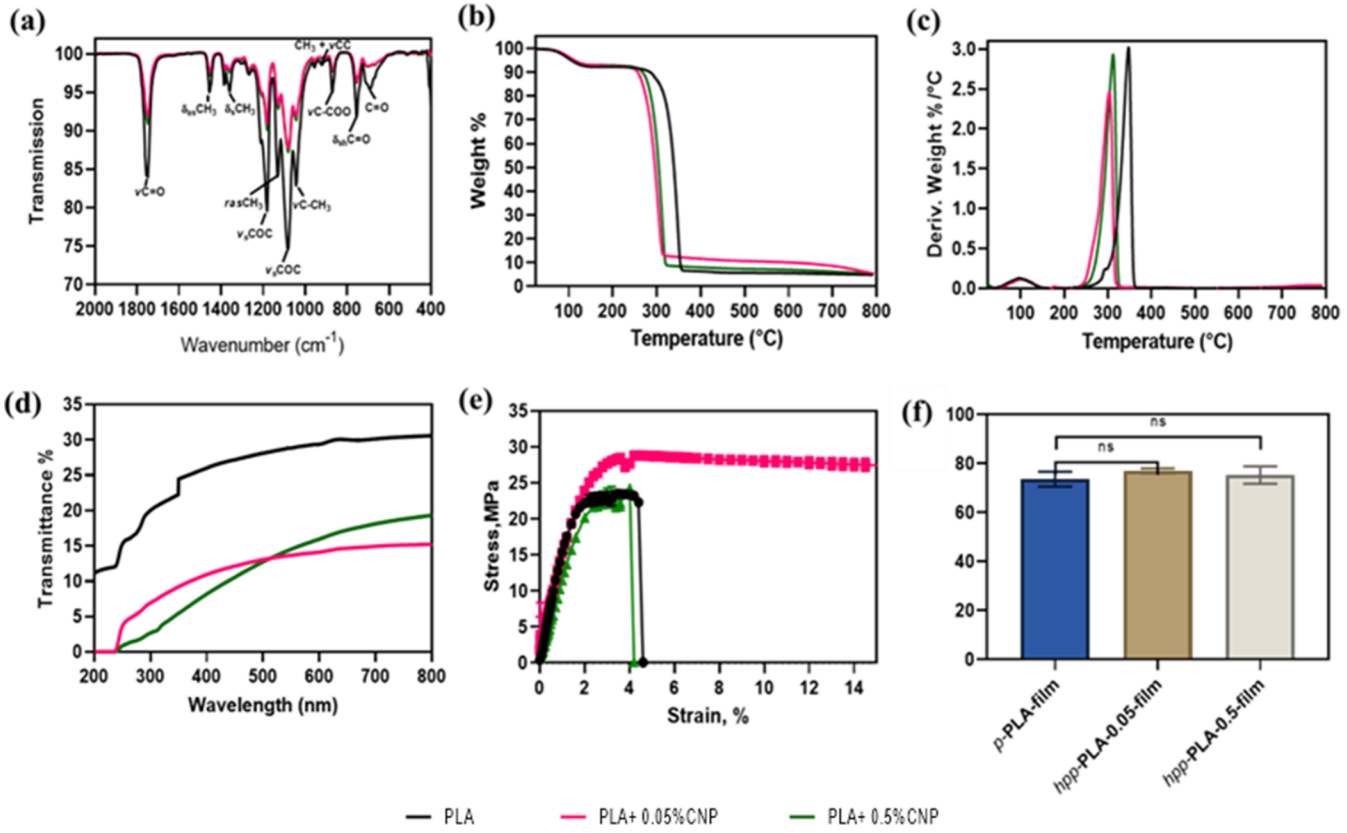


**Figure 1.** Characterization of carbon nanocomposite films with varying percentages of carbon nanoparticles. Representative (a) FTIR, (b) TGA, (c) derivative of TGA, (d) stress−strain curves, (e) UV−vis transmittance spectra, and (f) water contact angles of *p*-PLA-film and *hpp*-PLA-film samples. An ANOVA-based statistical analysis was performed among different samples to observe $p < 0.05$.

## 3. RESULTS AND DISCUSSION

Retaining the quality of food, pharmaceutical, or sustainability products for a longer timespan generally requires either optimum storing conditions or improvised packaging materials. The latter strategy has been endorsed superiorly in cases of sustainability products, which can be protected against natural harshness and physical, chemical, or radiational damages by using optimal packaging. Polymers, especially *p*-PLA, have been known for long to generate packaging films, but the lack of intrinsic antimicrobial properties, requirement of further strength, and need for improved biodegradability hamper their widespread use. Herein, we have developed intrinsically antibacterial polylactic acid films for high-performance packaging with optimally entangled carbon nanoparticles of biological origin. The synthesis methodologies are focused on the synthesis of *hf*-CNP from a carbon source, hemp fibers. Hemp is a fast-growing crop and is cost-effective due to its high output per acre and the capacity to grow in varied environments.[42] The common chemicals and compounds used are well-known for their efficacy in digesting cellulose, ensuring the high-quality manufacture of microcellulose. Many of these substances, such as hydrogen peroxide and ethanol, offer more environmentally friendly choices compared to harsher chemicals, lessening the environmental impact. The chemicals and compounds are readily available and cost-effective, making them ideal for industrial-scale uses. High-speed centrifugation is particularly advantageous in nanoparticle synthesis and purification due to numerous main features by successfully isolating nanoparticles based on size and density and effectively removing bigger aggregates or clusters. This technique also increases the quality of the final product by isolating nanoparticles from unreacted components, byproducts, and residual chemicals, leading to a pure and more consistent sample. Our goal is to create a commercially viable process that can be scaled up to industrial levels.

**3.1. Preparation and Characterization of *hf*-CNPs and *hpp*-PLA-Films.** Carbon nanoparticles were synthesized from hemp fibers using microwave-assisted hydrothermal synthesis and named *hf*-CNPs. The microwave hydrothermal method is preferred over the conventional hydrothermal method due to its attributes of a rapid heating rate, a sensitive reaction, and a uniform heating system.[43] The synthesized nanoparticles (*hf*-CNPs) were characterized by using dynamic light scattering to determine the distribution of hydrous particle size. The hydrodynamic diameter of *hf*-CNPs was found to be ∼104 nm with a polydispersity index of 0.2. The UV−visible spectra of *hf*-CNPs revealed a characteristic peak at around 350 nm, corresponding to $n-\pi^*$ transitions, which might have been generated due to the graphitic components of the carbon nanoparticles. The increase in the centrifugation speed had an impact on the average hydrodynamic diameter of the produced population of *hf*-CNPs. Probably, at a higher speed, lower diameter *hf*-CNPs were settled down and could be resuspended in ethanol, which was finally used for the preparation of packaging films (Figure S1).[44−46] Ethanol suspension of *hf*-CNPs was mixed with the chloroform solution of *p*-PLA and allowed to air-dry in controlled conditions at room temperature for 2 days to prepare *p*-PLA-films, *hpp*-PLA-0.05-film, and *hpp*-PLA-0.5-film, which were named based on the loaded percentage of *hf*-CNPs as 0,


https://doi.org/10.1021/acsomega.4c05732
ACS Omega 2024, 9, 45104−45116

0.05, and 0.5% (w/w), respectively. Prepared films were characterized by various physiochemical techniques to evaluate the enhanced properties after the entangling of *hf*-CNPs in *p*-PLA-films. The FTIR was used to study the molecular interaction between *p*-PLA and *hf*-CNPs in prepared *hpp*-PLA-films. In Figure 1a, peaks at 1748, 1359, and 870 $cm^{-1}$ can be observed due to the vibrational stretching of C═O, $\delta CH_3$ symmetric bending, $\nu$C−COO stretching, respectively, in the control *p*-PLA-film and produced samples of *hpp*-PLA-films. The peaks at 1455, 1130, and 1042 $cm^{-1}$ represent that asymmetric $\delta CH_3$ deformation, $rCH_3$ rocking, and the $\nu$C−$CH_3$ stretching mode in the *p*-PLA-film shift to lower wavenumbers of 1453, 1125, and 1041 $cm^{-1}$ in *hpp*-PLA-films, respectively.

The peaks at 1082 and 754 $cm^{-1}$ could be assigned to C−O−C stretching peaks and $\delta$C═O in-plane bending, which shifted to 1080 and 753 $cm^{-1}$ in *hpp*-PLA-film, whereas the peak at 691 $cm^{-1}$ depicting $\gamma$C═O out-of-plane bending in *p*-PLA-film disappeared in *hpp*-PLA-film (Table S3).[47,48] The absence of any additional peaks in the FTIR spectra of *hpp*-PLA-film compared to the *p*-PLA-film suggests that the chemical structure of *p*-PLA stays mostly unaltered following the incorporation of *hf*-CNPs and does not create any additional functional groups, thus preserving the original polymer structure. Further, the changes detected in specific peaks, such as the C═O stretching, $\delta CH_3$ bending, and vC−COO stretching modes, moving toward lower wavenumbers, suggest a modification in the molecular surroundings with the weakening of the bonds. The probable cause could be the interplay between *p*-PLA and the *hf*-CNPs. Shifts like these typically indicate alterations in chemical interactions, such as hydrogen bonding, which can impact the strength of the bond and the frequency of vibration. The observed changes in peak positions, particularly those associated with carbonyl and ester functional groups, indicate that *hf*-CNPs may be forming hydrogen bonds with *p*-PLA.

The thermal properties of packaging materials are generally examined to understand the robustness of packaging during the transport and storage processes. The thermal decomposition of *hpp*-PLA-films was studied by TGA and the derivative of TGA (Figure 1b,c). The *p*-PLA-film and *hpp*-PLA-films were found to be thermally degraded in a two-step process. The addition of *hf*-CNPs was found to not affect the onset degradation temperature (100 °C) with an 8% weight loss. The second degradation step resulted in ∼85, 78.25, and 82% weight loss in *p*-PLA-film, *hpp*-PLA-0.05-film, and *hpp*-PLA-0.5-film, respectively. It was noticed that *hpp*-PLA-films degraded at lower temperatures (302 and 311 °C) than *p*-PLA-film (348 °C). This decline in $T_{max}$ probably occurred due to the high specific surface area (SSA) of *hf*-CNPs entangled in *hpp*-PLA-films. High SSA is generally associated with the existing active sites and functional groups, which have the ability to interact with the polymer macromolecules, thereby causing a decrease in the thermal degradation temperature. Thus, the ability of *hf*-CNPs to act as a nucleating agent is probably responsible for this reduction, along with improved orderedness of *p*-PLA-film.[49] Plausibly, during the nucleation process, *p*-PLA chains interact with the *hf*-CNP surface with CH−$\pi$ interactions, followed by successive deposition of *p*-PLA polymer chains covering the surface of *hf*-CNP.[50] These interactions could vary for a lower loading amount of 0.05% *hf*-CNPs, where polymer chains in *p*-PLA are just perturbed with fewer nucleation centers. A higher loading amount of 0.5% results in the formation of agglomerates, causing significant structural disruptions to show considerable variation in various physical properties including thermal properties. Thus, the increased degradation temperature in *hpp*-PLA-0.5-film compared to *hpp*-PLA-0.05-film was due to these large agglomerates of *hf*-CNPs in *p*-PLA.[51] Overall, the decrease in the degradation temperature with the addition of *hf*-CNPs could be beneficial for the industrial thermal decomposition of the packaging material without any significant effect on the processing temperature range of *hpp*-PLA-films.

Further, the mechanical properties of *hpp*-PLA-films were examined using tensile tests (Figure 1d). The test showed that the incorporation of *hf*-CNPs in *p*-PLA (*hpp*-PLA-film) could reduce the brittleness, which was evident by the improved tensile strength and young modulus values. The advantageous interaction of hydrophilic functional groups in *p*-PLA and *hf*-CNPs probably improved the overall mechanical properties of the *hpp*-PLA-films. These improved mechanical properties were probably due to systematic load transfer between *hf*-CNPs to polymeric chains of *p*-PLA. It was observed that the tensile strength of *hpp*-PLA-0.5-film decreased compared to that of *hpp*-PLA-0.05-film from 28.7 to 24.6 MPa, which was still higher than the tensile strength of *p*-PLA-film (23.6 MPa, Table S2). As recorded, Young's modulus of *hpp*-PLA-0.05-film was 16.11 MPa, which was ∼66% higher than that of *p*-PLA-film and ∼47.4% higher than that of *hpp*-PLA-0.5-film.[52] These trends indicate that tensile and moduli increase with the entangling of *hf*-CNPs in the *p*-PLA-film but are not linear to the loaded % of *hf*-CNPs.[53] This indicates an increase in the brittleness of the *p*-PLA matrix at higher amounts of *hf*-CNPs with a decrease in mechanical strength, so probably higher loading might have led to a microstructural defect in *hpp*-PLA-films.[51] As increased tensile strength contributes toward maintaining the integrity of the packaging material to resist the stress condition during transport and storage, *hpp*-PLA-0.05-film might be the better packaging film compared to conventional *p*-PLA-films. The UV-vis radiation in the wavelength range of 280−315 nm is generally responsible for the photochemical degradation of materials of human use due to the high energy associated with it.[53] It has been reported that the *p*-PLA-film allows ∼28% of light to be transmitted in the visible range and ∼10% in the UV range, which can be significantly damaging to the products packaged inside and needs to be reduced further to make it a better packaging material. To improve packaging effectiveness, it is important to restrict this light transmission to a further significantly decreased level. It was found that incorporating *hf*-CNPs into *p*-PLA sheets moderately impaired light transmission. Specifically, *hpp*-PLA-0.05-film and *hpp*-PLA-0.5-film could reduce visible light transmission to 11% and 16%, respectively, compared to 28% in the *p*-PLA-film. The UV light transmission was also markedly reduced by these films, where *hpp*-PLA-0.05-film and *hpp*-PLA-0.5-film allowed only 2% and 6% transmission, respectively, which were significantly lower than the 10% transmission found through the *p*-PLA-film (Figure 1e). This reduction in transmitted radiation due to entangled *hf*-CNPs incorporated in the *p*-PLA-film might be due to optical absorption properties in the UV−vis range.[2851] The incorporation of carbonaceous fillers like *hf*-CNPs can partially block the light transmission over the UV−vis spectrum because *hf*-CNTs decrease the effective depth of UV penetration, thereby reducing the extent of polymer degradation.[54−56] Interestingly, 0.05% *hf*-CNPs were more effective at suppress-


https://doi.org/10.1021/acsomega.4c05732
ACS Omega 2024, 9, 45104−45116

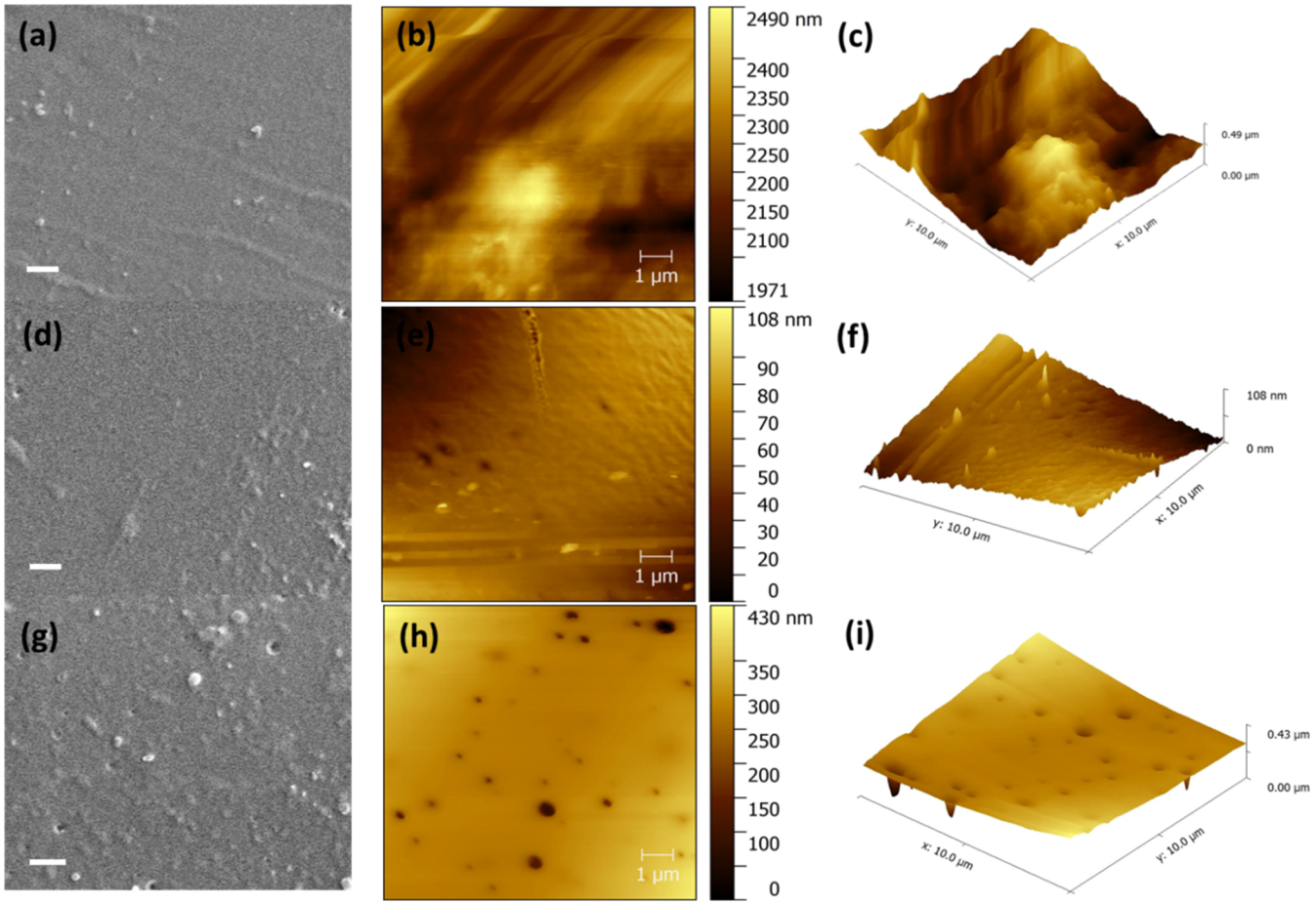


**Figure 2.** Surface topography of the *p*-PLA film and the impact of *hf*-CNP incorporation in *hpp*-PLA-0.05-film and *hpp*-PLA-0.5-film. The SEM images showcase the surface characteristics of (a) *p*-PLA-film, (d) *hpp*-PLA-0.05-film, and (g) *hpp*-PLA-0.5-film with a scale bar of 2 $\mu$m. Additionally, AFM images provide surface roughness details, displaying both 2D and 3D representations for each film: (b) and (c) *p*-PLA, (e) and (f) *hpp*-PLA-0.05, and (h) and (i) *hpp*-PLA-0.5.

ing visible light than 0.5% *hf*-CNPs. This may be because 0.5% *hf*-CNPs are less uniformly distributed, resulting in a larger fraction of the *hpp*-PLA-0.5-film remaining as unaffected PLA.

The aqueous wettability of packaging materials is another important parameter to establish its superiority.[57−59] This property can be evaluated by calculating the water contact angle of the films. As depicted in Figure 1f, the *p*-PLA-film surface was hydrophilic with a contact angle of 73.7°, whereas the addition of 0.05 and 0.5% *hf*-CNPs slightly increased it to ∼77° and 75°, respectively, with increased hydrophobicity. The ANOVA-based statistical analysis results indicated that there was no statistically significant difference in the water contact angles between the *hpp*-PLA-0.05-film and *hpp*-PLA-0.5-film when compared with the *p*-PLA-film, with $P$ <0.05. This shows that the integration of *hf*-CNPs at these percentages did not noticeably modify the surface hydrophobicity of the *hpp*-PLA-films in comparison to that of the *p*-PLA-film samples (Figure 1f)

Scanning electron microscopy images revealed surface topographical differences between the *p*-PLA-film and *hpp*-PLA-films into which *hf*-CNPs were incorporated (Figure 2). The *p*-PLA-film (Figure 2a) exhibited a relatively uneven surface, while *hpp*-PLA-0.05-films (Figure 2d) modified with a lower amount of *hf*-CNPs improved the evenness but in *hpp*-PLA-0.5-film, and unevenness was improved further, probably due to agglomerations (Figure 2g) of a higher percentage of *hf*-CNPs loaded in this film.[60,61] The AFM method was used to determine the dimensions and texture of *hpp*-PLA-films, concentrating on the interaction between surface morphology and surface chemistry and giving rise to surface effects.[62] The uneven surface texture observed in the *p*-PLA-film can be attributed to the intrinsic properties of *p*-PLA and the conditions under which it is processed. Variability in surface texture in the *p*-PLA-film is often influenced by factors such as the film's thickness, cooling rates during production, and residual stresses from the manufacturing process. The AFM approach offered measurements of roughness metrics, including $S_a$ (average roughness), $S_q$ (root-mean-square roughness), and $S_{dq}$ (surface slope). The roughness parameters for *p*-PLA, specifically $S_a$, $S_q$, and $S_{dq}$, were recorded at 614.2 nm, 732 nm, and 0.395, respectively. The experiment revealed the impact of adding *hf*-CNPs into *p*-PLA, testing two percentages (0.05 and 0.5%). The addition of 0.05% *hf*-CNPs considerably lowered the roughness values to 380.3 nm, 462.8 nm, and 0.233, respectively, showing a much smoother surface compared to *p*-PLA. However, with 0.5%, the roughness values increased to 594.6 nm, 760 nm, and 0.308, respectively, considerably higher than those in the case of 0.05% and still lower than those of *p*-PLA. These results imply that adding *hf*-CNsP can affect the surface roughness of *hpp*-PLA-films, with the lower percentage being more efficient in producing smoothness. A balanced *hf*-CNP content appears to


https://doi.org/10.1021/acsomega.4c05732
ACS Omega 2024, 9, 45104−45116

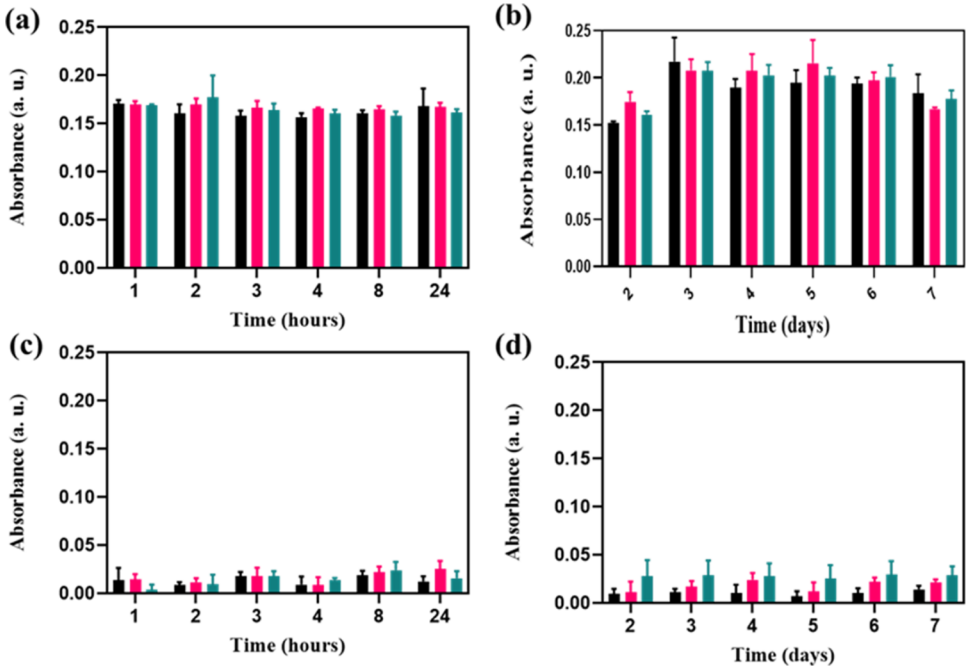


**Figure 3.** Dissolution study of *hpp*-PLA-films at different time intervals in water: (a) short-term (24 h) and (b) long-term (7 days) and in PBS buffer at pH = 8.5 with (c) short-term (24 h) and (d) long-term (7 days).

be important to maximize surface qualities. Thus, these findings exhibit that surface roughness decreases in *hpp*-PLA-films (Figure 2e,f,h,i) in comparison to the *p*-PLA-film (Figure 2b,c). The surface roughness is lower in *hpp*-PLA-0.05-film than that in *hpp*-PLA-0.5-film. Probably, the inclusion of *hf*-CNPs in *p*-PLA facilitated surface smoothness.

The TEM images offer compelling visual evidence indicating the uniform dispersion of *hf*-CNPs within the polymer matrix of *p*-PLA in the prepared *hpp*-PLA-0.05-film. This even distribution is apparent at various magnification levels, which shows the consistency of nanoparticle integration across the polymer layer (Figure S3). At lower magnifications, the TEM pictures offer a comprehensive overview of the polymer matrix (Figure S3a) and distribution *hf*-CNPs across *hpp*-PLA-0.05-film (Figure S3b), indicating a homogeneous distribution of *hf*-CNPs in PLA. At higher magnification levels, the spheroidal morphology of individual *hf*-CNPs could also be seen and realized for being conveniently entangled within the *p*-PLA matrix (Figure S3d), while the *p*-PLA-film showed no sign of *hf*-CNPs (Figure S3c).

**3.2. Dissolution Studies of *hpp*-PLA-Films in Water and Regulated pH Conditions.** The release of efficiency-improving contents like nanodopants from packaging films has always been a concern for the quality of packaged materials, as released dopants can get integrated into packaged materials and contaminate the material or contaminate the surrounding. Thus, a no-to-lower or nonconsequential release of dopants would be a preferential property for a better packaging film. To investigate these possibilities, produced *hpp*-PLA-films were investigated for dissolution in water or other possible pH conditions. During the dissolution study under water and pH conditions, the *p*-PLA-film and *hpp*-PLA-films were tested in triplicate to ensure the reliability and reproducibility of the results. Here, dissolution studies were carried out to evaluate the probable release of *hf*-CNPs from *hpp*-PLA-films in normal water and different pH conditions.[39,63] Phosphate-buffered saline (PBS) was chosen to imitate a stable, biologically relevant environment because it maintains a steady pH value and ionic strength. This selection ensures proper assessment of the material's dissolution behavior, making the results credible and comparable to biological system conditions. The release was estimated by recording the absorption spectra between 200 to 800 nm after submerging the films in water and a pH 8.5 buffer to replicate the conditions where *hpp*-PLA-films would be exposed to floodwater. The short- and long-term dissolution up to 24 h (Figure 3a) and 7 days (Figure 3b), respectively, for *p*-PLA-film and *hpp*-PLA-films in water was found to be comparable with no added effects from *hf*-CNPs loaded either in a lower amount (*hpp*-PLA-0.05-film) or in a higher amount (*hpp*-PLA-0.5-films; Figure 3b). Similarly, the short- and long-term dissolution of films in PBS at pH 8.5 (Figure 3c,d) did not show any clear difference in the absorption pattern. However, it was noticeable that overall dissolution for the *p*-PLA-film itself was considerably higher in water compared to the buffer of pH 8.5, which was not affected by the inclusion of *hf*-CNPs either in lower or higher percentages. Thus, it can be concluded that *hf*-CNPs leached from *hpp*-PLA-films while being submerged in water and buffer (pH 8.5) even up to 7 days were insignificant, and thus, produced *hpp*-PLA-films are comparatively good packaging films.

**3.3. Antibacterial Properties of *hpp*-PLA-Films.** The antibacterial properties of *hpp*-PLA-films were measured against Gram-positive *Bacillus subtilis* and Gram-negative *E. coli*. *Escherichia coli* and *Bacillus subtilis* were chosen for this investigation to contain both Gram-negative (*E. coli*) and Gram-positive (*B. subtilis*) bacteria in the spectrum of antibacterial studies. Moreover, their ubiquitous presence in nature makes them extremely important and useful for such study. This work aims to assess the antimicrobial properties of *hpp*-PLA sheets against commonly found bacteria and investigate the underlying processes responsible for their


https://doi.org/10.1021/acsomega.4c05732
ACS Omega 2024, 9, 45104−45116

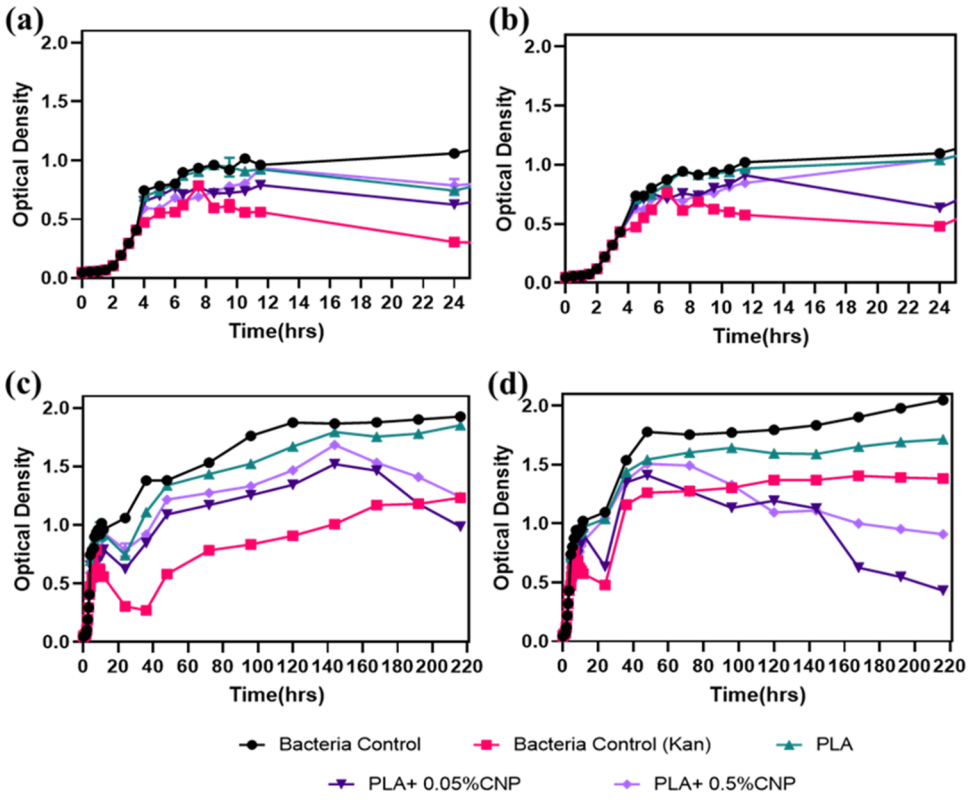


**Figure 4.** Antibacterial properties of *p*-PLA and *hpp*-PLA-films after incubation for (a, b) short-term and (c, d) long-term tested against (a, c) Gram-positive *B. subtilis* and (b, d) Gram-negative *E. coli* with varying percentages of *hf*-CNPs. The antibiotic kanamycin was used as a positive control.

antibacterial activity. The ability of *hpp*-PLA-films to reduce the growth of bacteria in optimum conditions was analyzed for 10 days at different intervals (Figure 4). As *p*-PLA-films are known to have no antibacterial properties, any decrease in bacterial growth could be associated with the incorporation of *hf*-CNPs. The antibacterial characteristics of *hf*-CNPs are derived from their starting material, hemp fibers. The antibacterial properties of hemp may be associated with alkaloids and phenolic compounds present in lignin.[64−67] The optical density of bacterial suspensions in the presence of *p*-PLA-film and *hpp*-PLA-films at different intervals depicts the antibacterial effect of *hf*-CNPs on the growth of the bacteria. Probably, the intrinsic property of *hf*-CNPs caused the growth inhibition in both used experimental microorganisms, *E. coli* and *B. subtilis*. It was noticed that films were more effective against *E. coli* and *B. subtilis*, especially for long-term antibacterial studies. More interestingly, even when the positive control of kanamycin started losing its antibacterial effect at longer time points, *hf*-CNPs kept inhibiting the growth of both organism types, i.e., *E. coli* and *B. subtilis*. The percentage errors in the optical density measurement for *E. coli* and *B. subtilis* are 1.87 and 1.90, respectively.

To further establish the role of *hf*-CNPs as an antibacterial component of *hpp*-PLA-films, the samples were tested with *E. coli* and *B. subtilis*. The bacterial cells were incubated with *hpp*-PLA-films with different percentages of *hf*-CNPs, and the reduction in cell number was compared along with cells treated with kanamycin as a positive control (Figure S4). After 20 h of treatment with *hpp*-PLA-0.05-film, *E. coli* cell counts were reduced by 0.22 ± 0.003 log. A similar but somewhat smaller reduction was seen with the *hpp*-PLA-0.5-film, which resulted in a 0.13 ± 0.015 log reduction (Figure S4a). In comparison, treatment with kanamycin resulted in much reduced *E. coli* cell counts, with a drop of 0.54 ± 0.009 log. There was no substantial antibacterial impact detected with *p*-PLA-film alone, which supports the notion that *hf*-CNPs are responsible for the observed antibacterial activity. In an extended treatment of 212 h, both *hpp*-PLA-0.05-film and *hpp*-PLA-0.5-film demonstrated significantly higher reductions in *E. coli* cell counts. The *hpp*-PLA-0.05-film achieved a reduction of 0.29 ± 0.003 log, while the *hpp*-PLA-0.5-film resulted in a 0.19 ± 6.05 × $10^{-05}$ log reduction, both of which exceeded the reduction seen with kanamycin treatment (0.19 ± 0.03 log, Figure S4c).

After 20 hrs of treatment with *hpp*-PLA-0.05-film, *B. subtilis* cell counts were reduced by 0.23 ± 0.001 log. A smaller reduction was seen with the *hpp*-PLA-0.5-film, which resulted in a 0.020 ± 0.003 log reduction (Figure S4b). In comparison, treatment with kanamycin resulted in much reduced *B. subtilis* cell counts, with a drop of 0.36 ± 0.0007 log. There was no substantial antibacterial impact detected with *p*-PLA-film alone, which supports the notion that *hf*-CNPs are responsible for the observed antibacterial activity. In an extended treatment of 212 h, both *hpp*-PLA-0.05-film and *hpp*-PLA-0.5-film demonstrated significantly higher reductions in *B. subtilis* cell counts. The *hpp*-PLA-0.05-film achieved a reduction of 0.67 ± 0.003 log, while the *hpp*-PLA-0.5-film resulted in a 0.35 ± 0.003 log reduction, both of which exceeded the reduction seen with kanamycin treatment (0.17 ± 0.003 log, Figure S4d). These findings demonstrate that the presence of *hf*-CNPs in *hpp*-PLA-films is necessary for their antibacterial action. Over an extended period, the antibacterial


https://doi.org/10.1021/acsomega.4c05732
ACS Omega 2024, 9, 45104−45116

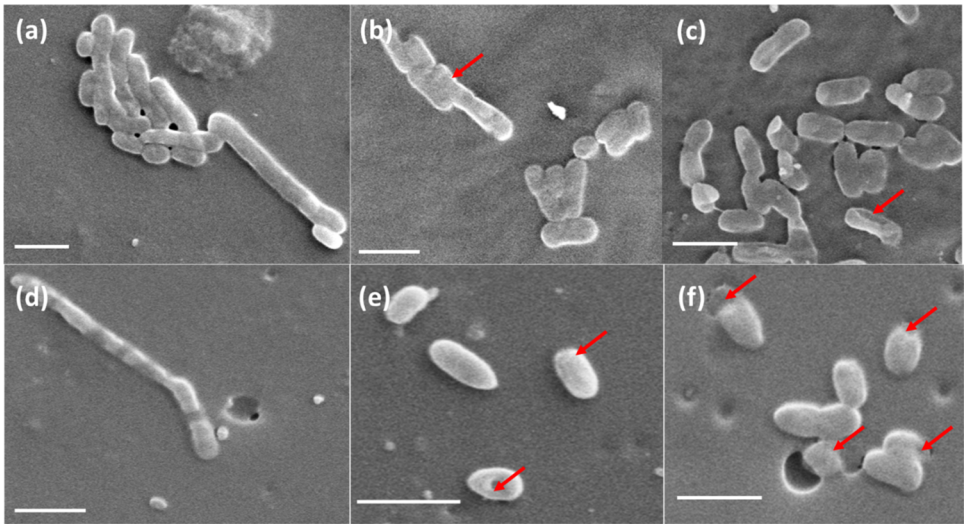


**Figure 5.** Scanning electron microscopy images of bacteria *E. coli* (a−c) and *B. subtilis* (d−f) on *p*-PLA and *hpp*-PLA-films. Arrows point to the damaged areas of cell walls on bacterial cells. Here, bacterial cells were incubated on (a, d) *p*-PLA-film, (b, e) *hpp*-PLA-0.05-film, and (c, f) *hpp*-PLA-0.5-film (scale bar: 2 $\mu$m).

effectiveness of *hpp*-PLA-films surpasses that of kanamycin, demonstrating the potential of *hpp*-PLA-films as a potent antibacterial material.[68]

To understand the effect of *hpp*-PLA-films on the bacterial population, electron microscopy was performed to scan the film surfaces. Collected scanning electron microscopy images revealed the changed morphology of bacteria on interaction with *hpp*-PLA-films (Figure 5). Figure 5a,d shows unmarred cells (*E. coli* and *B. subtilis*) on the *p*-PLA-film surface. As a result of incubation, the cell wall deformation in *E. coli* on *hpp*-PLA-0.05-films (Figure 5b) and *hpp*-PLA-0.5-films (Figure 5c) was observed, whereas *B. subtilis* were observed with deep indentations on *hpp*-PLA-0.05-film (Figure 5e) and *hpp*-PLA-0.5-film (Figure 5f). The size reduction was also observed in bacteria exposed to *hpp*-PLA-films.[69−72] These results indicate that *hpp*-PLA-0.05-film is better than *p*-PLA-film in damaging the morphology of the microbial cells, probably due to the presence of *hf*-CNPs, which are intrinsically antibacterial due to their origin from hemp fibers. In addition to morphological alterations, there was also a noticeable reduction in bacterial size for both *E. coli* and *B. subtilis* when exposed to *hpp*-PLA-films.[69−72] These data indicate that the *hpp*-PLA-films not only limit bacterial growth but also actively alter bacterial cell structures, resulting in considerable physical damage.[73] These observations show that probably contact-based antibacterial action is at play, as the antibacterial agent directly interacts with the bacterial cell membrane, affecting its structure and physiological functioning. The *hpp*-PLA-films, therefore, appear to efficiently degrade bacterial morphology and viability through direct contact, underlining their potential as effective antibacterial packaging materials.[73]

Scanning electron microscopy images were further analyzed with fluorescence mapping, revealing changed shape, size, and topography of bacterial cells upon interaction with *hpp*-PLA-films (Figure S5). Figure S5a,d represents the intact cells of *E. coli* and *B. subtilis* on the *p*-PLA-film surface, respectively. However, after incubation, cell wall deformation was detected in *E. coli* on *hpp*-PLA-0.05-film (Figure S5b) and *hpp*-PLA-0.5-film (Figure S5c), whereas *B. subtilis* exhibited deep indentations on *hpp*-PLA-0.05-film (Figure S5e) and *hpp*-PLA-0.5-film (Figure S5f). In addition to these morphological changes, a reduction in the bacterial size was reported for both *E. coli* and *B. subtilis* when exposed to *hpp*-PLA-films (Figure S6). These findings indicate that *hpp*-PLA-films not only limit bacterial growth (Figure 5) but also cause severe physical damage and a reduction in cell size (Figure S6). This shows that the films exhibit a contact-based antibacterial activity, physically engaging with the bacterial cell wall membrane and altering its structure and physiological processes.

It is important to study the feasibility of using these films in wrapping sophisticated shapes of various objects without breaking or creating permanent folds. Interestingly, all of the film samples (*p*-PLA-film, *hpp*-PLA-0.05-film, and *hpp*-PLA-0.5-film) were equally easy to wrap a model product, pocket water filtration cartridge (Figure S2), without any visible deformity. The only noticeable change was in transparency, where the inclusion of *hf*-CNPs had reduced the transparency of *hpp*-PLA-0.05-film and *hpp*-PLA-0.5-film.

Further, it was important to evaluate the cushioning efficiency of produced *hpp*-PLA-films.[74,75] The drop test can facilitate observing such efficiency where damages on the body of the object are observed after it is exposed to a heavy physical impact. To simulate the drop condition, a sand-filled transparent plastic bottle-like object of around 0.5 kg was wrapped in different film samples before they were dropped from a height of 80 feet. It was found that *hpp*-PLA-films impede the damage caused by the fall of the wrapped object compared to *p*-PLA-film (Figure 6a,b). This effect was more prominent in the wrapping of *hpp*-PLA-0.05-film than in the wrapping of *hpp*-PLA-0.5-film. It was probably possible due to the higher modulus and tensile strength of *hpp*-PLA-0.05-film, which allowed it to sustain more physical impact than both *hpp*-PLA-0.5-film and *p*-PLA-film.

Environmental remediation of polymeric products has always been the main goal for researchers and manufacturers. Establishing the improvised degradation of packaging films with certain control due to added dopants can be of high importance. Among many of the possible degradation modes, biodegradation carries high significance due to its less complex procedure, economical arrangements, and functional suitabil-


https://doi.org/10.1021/acsomega.4c05732
ACS Omega 2024, 9, 45104−45116

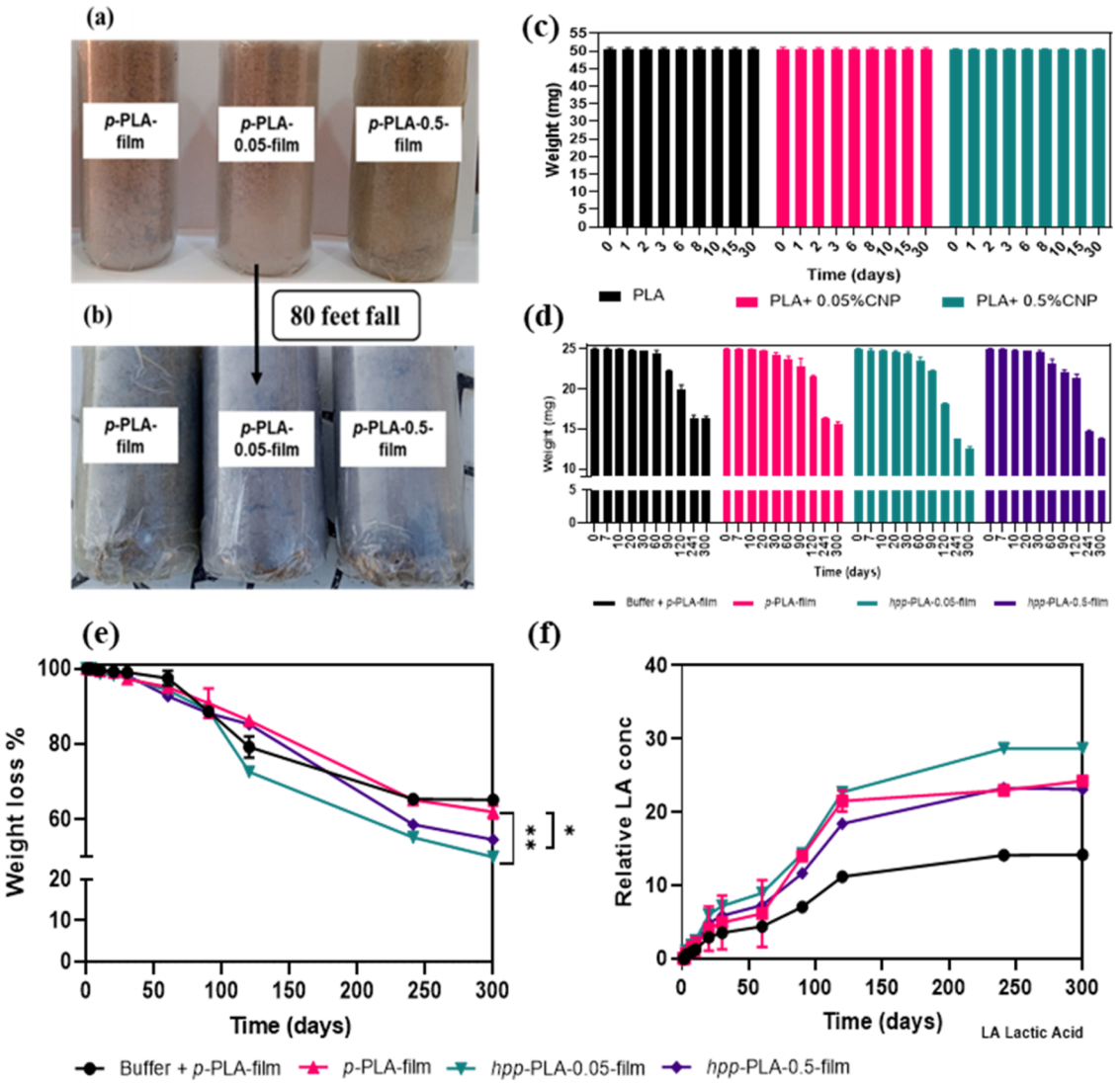


**Figure 6.** Physical impact and biodegradation response of the prepared films. The photographic images of wrapped objects (a) before and (b) after the drop. Biodegradation of films evaluated as (c) loss of weight under composting conditions; (d) weight loss and (e) relative weight loss percentage measured during enzymatic degradation in the presence of lipase. The statistical significance between *p*-PLA- and *hpp*-PLA-films was analyzed through ANOVA analysis (* = $P < 0.05$; ** = $P < 0.01$). (f) Evaluation of enzymatic biodegradation by relative lactic acid concentration measurement using UV−vis absorption against incubation time.

ity. Hence, we evaluated the biodegradability of developed films under more than one possible scenario, i.e., in compost and enzymatic suspension, mimicking the condition of an uncontrolled discard site and controlled degradation plant. It was found that for up to 30 days, no significant change in the weight of PLA films was seen in compost conditions, which did not get affected by the addition of *hf*-CNPs, indicating a reasonably stable nature of the films (Figure 6c).

The enzymatic degradation of *hpp*-PLA-films was followed by weight measurement and weight loss determination (Figure 6d). Though, at shorter time points, there was no noticeable weight loss in the lipase-degraded *p*-PLA- and *hpp*-PLA-films, time points of 7, 10, and 20 days revealed the incremental loss of films. It was interesting to note that the weight loss of *hpp*-PLA-0.05-film was around 2-fold higher than *p*-PLA-film with $p = 0.0505$ on performing an ANOVA test, whereas *hpp*-PLA-0.5-film degraded to a lesser extent on a longer time point of 20 days (Figure 6e). The experiment spanned 300 days, and the weight loss was recorded after 30, 60, 90, 120, 241, and 300 days. The results show that a modest amount of *hf*-CNPs can efficiently expedite the breakdown of the polymer matrix, whereas a higher percentage of *hf*-CNPs (0.5%) resulted in reduced deterioration of *hpp*-PLA-films. This implies that an excessive amount of nanoparticles may delay the degrading process, possibly due to changes in the film's structure, such as nanoparticle aggregation or altered physical properties. The enhanced degradation at a lower *hf*-CNP percentage shows that a more uniform dispersion of nanoparticles inside the polymer matrix is desirable. In contrast, a higher percentage may lead to less effective dispersion and reduced degradation efficiency (Figure 6e). The statistical significance between *p*-PLA- and *hpp*-PLA-films was analyzed through ANOVA analysis, which revealed that weight loss was significantly greater in *hpp*-PLA-0.05-film compared to those in *hpp*-PLA-0.5-film and *p*-PLA-film. It was interesting to note that the weight loss of *hpp*-PLA-0.05-film was around 2-fold higher than that of *p*-PLA-film with $p = 0.0505$ on performing a *t*-test, whereas *hpp*-PLA-0.5-film degraded to a lesser extent in a


https://doi.org/10.1021/acsomega.4c05732
ACS Omega 2024, 9, 45104−45116

longer time point of 20 days (Figure 6e). The results show that weight loss was improved with addition of 0.05% of *hf*-CNPs, while a higher percentage slowed down the overall degradation. Alternatively, degradation was followed by estimating the released amount of lactic acid from films being incubated with lipase enzyme. After calibration ($\varepsilon_{390\ nm}$ = 17.611 $dm^3\ mol^{-1}\ cm^{-1}$), the generated lactic acid could be translated into weight loss, and this computed weight loss was displayed versus degradation time (Figure 6f). The method relies on the reaction between iron(III) chloride and lactate ions, which are components of lactic acid. This interaction produces a colored product of iron lactate. The results show that the inclusion of *hf*-CNPs increased the degradation of *hpp*-PLA-0.05-film compared to *p*-PLA-film. However, a higher *hf-CNP* content in *hpp*-PLA-0.5-film did not facilitate the process and reduced the extent of degradation. Probably, the better distribution of the lower percentage of *hf*-CNPs in *hpp*-PLA-0.05-film was responsible for higher degradation than lower degradation in the case of a 10-fold higher concentration in *hpp*-PLA-0.5-film, whereas the absence of *hf*-CNPs makes it less degradable, as expected.

## 4. CONCLUSIONS

Storage conditions and packaging materials are optimized to preserve the integrity of food, drugs, or sustainable products. The latter approach is preferred by sustainable products because it protects them from the external environment. Although polymers such as *p*-PLA have been used in packaging applications due to some biodegradability, their susceptibility to bacterial contamination raises serious concerns. In this study, carbon nanoparticles of biological origin have been used to create high-performance polylactic acid films that are inherently antibacterial with higher biodegradability. Here, the properties of *p*-PLA have been improved by using *hf*-CNPs, an inherently antibacterial agent synthesized from hemp fibers. The prepared *hf*-CNPs could be successfully used as nucleating agents in *hpp*-PLA-films. This ultimately leads to a decreased $T_{max}$ and improved load sharing. It was also found to be better in terms of UV−visible radiation absorption and increased surface smoothness. The limited leaching of *hf*-CNPs from the films under varied situations established it as a low-risk packaging for contaminating the packaged products or the surrounding environment. Despite the fact that *p*-PLA-films have no antibacterial properties, *hpp*-PLA-films showed antibacterial effects based on contact-based inhibition in cases of *E. coli* and *B. subtilis*, with long-lasting effects surpassing even kanamycin at longer time points. Further, a successful drop test reveals that *hpp*-PLA-films could offer adequate cushioning, making them suitable for protecting contents during handling and transit. Additionally, the improved biodegradability of *hpp*-PLA-films compared to *p*-PLA- films, especially with a 0.05% *hf*-CNP loading, suggests that these films are suitable for environmental sustainability while giving an enhanced packaging performance. Based on the obtained results, it can be concluded that *hpp*-PLA-0.05-film could be a better alternative for PLA-based packaging films and can be used in the packaging industry.

## ASSOCIATED CONTENT

### Supporting Information

The Supporting Information is available free of charge at https://pubs.acs.org/doi/10.1021/acsomega.4c05732.

Effect of centrifugation speed on separation of *hf*-CNPs; photographic images of films wrapped on a model product to be used in flooded areas for purification of water; list of antibacterial polymeric packaging materials; ultimate tensile strength and Young's modulus studies; analysis of functional groups in the *p*-PLA-film and *hpp*-PLA-films using the FTIR spectrum; and experimental details (PDF)

## AUTHOR INFORMATION


### Corresponding Author

**Santosh K. Misra** − *Department of Biological Sciences & Bioengineering, Indian Institute of Technology Kanpur, Kalyanpur, UP 208016, India; The Mehta Family Centre for Engineering in Medicine, Indian Institute of Technology Kanpur, Kalyanpur, UP 208016, India;* orcid.org/0000-0002-3313-4895; Phone: +91-512-679-4013; Email: skmisra@iitk.ac.in

### Authors

**Neha Yadav** − *Department of Biological Sciences & Bioengineering, Indian Institute of Technology Kanpur, Kalyanpur, UP 208016, India; Directorate of Nanomaterials, Defence Materials & Stores Research & Development Establishment (DMSRDE), Kanpur, UP 208013, India*

**Debmalya Roy** − *Directorate of Nanomaterials, Defence Materials & Stores Research & Development Establishment (DMSRDE), Kanpur, UP 208013, India;* orcid.org/0000-0003-3629-5309

Complete contact information is available at: https://pubs.acs.org/10.1021/acsomega.4c05732


### Notes

The authors declare no competing financial interest.

## ACKNOWLEDGMENTS

The authors would like to acknowledge the financial support of the Defence Materials & Stores Research & Development Establishment (DMSRDE), Kanpur (Project No. 2019130). The authors would like to acknowledge facilities offered by Advanced Center for Materials Science, Indian Institute of Technology Kanpur and Directorate of Nanomaterials, Defence Materials & Stores Research & Development Establishment (DMSRDE), Kanpur

## REFERENCES


(1) Reverte, J. M.; Caminero, M. Á.; Chacón, J. M.; García-Plaza, E.; Núñez, P. J.; Becar, J. P. Mechanical and Geometric Performance of PLA-Based Polymer Composites Processed by the Fused Filament Fabrication Additive Manufacturing Technique. *Materials* **2022**, *13*, 1924 DOI: 10.3390/ma13081924.

(2) Rai, P.; Mehrotra, S.; Priya, S.; Gnansounou, E.; Sharma, S. K. Recent Advances in the Sustainable Design and Applications of Biodegradable Polymers. *Bioresour. Technol.* **2021**, *325*, No. 124739.

(3) Ghosh, K.; Jones, B. H. Roadmap to Biodegradable Plastics—Current State and Research Needs. *ACS Sustainable Chem. Eng.* **2021**, *9* (18), 6170−6187.

(4) Fahmy, H. M.; Salah Eldin, R. E.; Abu Serea, E. S.; Gomaa, N. M.; AboElmagd, G. M.; Salem, S. A.; Elsayed, Z. A.; Edrees, A.; Shams-Eldin, E.; Shalan, A. E. Advances in Nanotechnology and Antibacterial Properties of Biodegradable Food Packaging Materials. *RSC Adv.* **2020**, *10* (35), 20467−20484.

(5) Ebrahimi, F.; Ramezani Dana, H. Poly Lactic Acid (PLA) Polymers: From Properties to Biomedical Applications. *Int. J. Polym. Mater. Polym. Biomater.* **2022**, *71* (15), 1117−1130.
(6) Divakara Shetty, S.; Shetty, N. Investigation of Mechanical Properties and Applications of Polylactic Acids - A Review. *Mater. Res. Express* **2019**, *6*, 112002 DOI: 10.1088/2053-1591/ab4648.
(7) Lunt, J. Large-Scale Production, Properties and Commercial Applications of Polylactic Acid Polymers. *Polym. Degrad. Stab.* **1998**, *59* (1), 145−152.
(8) Kain, S.; Ecker, J. V.; Haider, A.; Musso, M.; Petutschnigg, A. Effects of the Infill Pattern on Mechanical Properties of Fused Layer Modeling (FLM) 3D Printed Wood/Polylactic Acid (PLA) Composites. *Eur. J. Wood Prod.* **2020**, *78* (1), 65−74.
(9) Misra, S. K.; Srivastava, I.; Tripathi, I.; Daza, E.; Ostadhossein, F.; Pan, D. Macromolecularly "Caged" Carbon Nanoparticles for Intracellular Trafficking via Switchable Photoluminescence *J. Am. Chem. Soc.* 2017, DOI: 10.1021/jacs.6b11595.
(10) Lei, Y.; Mao, L.; Yao, J.; Zhu, H. Improved Mechanical, Antibacterial and UV Barrier Properties of Catechol-Functionalized Chitosan/Polyvinyl Alcohol Biodegradable Composites for Active Food Packaging. *Carbohydr. Polym.* **2021**, *264*, No. 117997.
(11) Misra, S. K.; Srivastava, I.; Tripathi, I.; Daza, E.; Ostadhossein, F.; Pan, D. Macromolecularly "Caged" Carbon Nanoparticles for Intracellular Trafficking via Switchable Photoluminescence. *J. Am. Chem. Soc.* **2017**, *139* (5), 1746−1749.
(12) Aziman, N.; Abdullah, N.; Bujang, A.; Mohd Noor, Z.; Abdul Aziz, A.; Ahmad, R. Phytochemicals of Ethanolic Extract and Essential Oil of Persicaria Hydropiper and Their Potential as Antibacterial Agents for Food Packaging Polylactic Acid Film. *J. Food Saf.* **2021**, *41* (1), e12864 DOI: 10.1111/jfs.12864.
(13) Morena, A. G.; Tzanov, T. Antibacterial Lignin-Based Nanoparticles and Their Use in Composite Materials. *Nanoscale Adv.* **2022**, *4*, 4447−4469, DOI: 10.1039/d2na00423b.
(14) Sanguyo, F. H. C.; Angeles, F. L. A.; Deborde, S. M. V.; Jumarang, K. C.; Mahait, J. A.; Onayan, R. S. M.; Pacada, M. J. V.; Pitong, C. R.; Hagosojos, B. M. Bacteriocin and Its Current Application as a Food Packaging Film Component against Spoilage: A Narrative Review. *Asian J. Biol. Life Sci.* **2021**, *10* (2), 325−339.
(15) Ordoñez, R.; Atarés, L.; Chiralt, A. Effect of Ferulic and Cinnamic Acids on the Functional and Antimicrobial Properties in Thermo-Processed PLA Films. *Food Packag Shelf Life* **2022**, *33*, No. 100882.
(16) Turalija, M.; Bischof, S.; Budimir, A.; Gaan, S. Antimicrobial PLA Films from Environment Friendly Additives. *Compos B Eng.* **2016**, *102*, 94−99.
(17) Bisht, D.; Faujdar, S. S.; Sharma, A. Antibacterial Potential of Neem (Azadirachta Indica) against Uropathogens Producing Beta-Lactamase Enzymes: A Clue to Future Antibacterial Agent? *Biomed. Biotechnol. Res. J. (BBRJ)* **2020**, *4* (3), 232 DOI: 10.4103/bbrj.bbrj_38_20.
(18) Gootz, T. D.; Barrett, J. F.; Sutcliffe, J. A. Inhibitory Effects of Quinolone Antibacterial Agents on Eucaryotic Topoisomerases and Related Test Systems. *Antimicrobial Agents Chemotherapy* **1990**, *34*, 8−12, DOI: 10.1128/aac.34.1.8.
(19) Kawakami, H.; Inuzuka, H.; Hori, N.; Takahashi, N.; Ishida, K.; Mochizuki, K.; Ohkusu, K.; Muraosa, Y.; Watanabe, A.; Kamei, K. Inhibitory Effects of Antimicrobial Agents against Fusarium Species. *Med. Mycol* **2015**, *53* (6), 603−611.
(20) Shao, L.; Xi, Y.; Weng, Y. Recent Advances in PLA-Based Antibacterial Food Packaging and Its Applications. *Molecules* **2022**, *27*, 5953 DOI: 10.3390/molecules27185953.
(21) Khan, M. S.; Misra, S. K.; Dighe, K.; Wang, Z.; Schwartz-Duval, A. S.; Sar, D.; Pan, D. Electrically-Receptive and Thermally-Responsive Paper-Based Sensor Chip for Rapid Detection of Bacterial Cells. *Biosens. Bioelectron.* **2018**, *110*, 132 DOI: 10.1016/j.bios.2018.03.044.
(22) Shojaeiarani, J.; Shirzadifar, A.; Shine, C.; Reisi, A. M. Hybrid Nanocomposite Packaging Films from Cellulose Nanocrystals, Zinc Sulfide Quantum Dots Reinforced Polylactic Acid with Fluorescent and Antibacterial Properties. *Polym. Eng. Sci.* **2022**, *62* (5), 1562−1570.
(23) Chong, W. J.; Shen, S.; Li, Y.; Trinchi, A.; Pejak Simunec, D.; Kyratzis, I. Louis.; Sola, A.; Wen, C. Biodegradable PLA-ZnO Nanocomposite Biomaterials with Antibacterial Properties, Tissue Engineering Viability, and Enhanced Biocompatibility. *Smart Mater. Manufacturing* **2023**, *1*, No. 100004.
(24) Nabgui, A.; Follain, N.; Vidović, E.; El Haskouri, J.; Marais, S.; El Meziane, A.; Lahcini, M.; Thébault, P. Preparation and Study of the Thermal, Barrier and Antibacterial Properties of Polylactic Acid-Fluorphlogopite-Silver Nanoparticles Nanocomposite Films. *Prog. Org. Coat.* **2022**, *171*, No. 107041.
(25) Akshaykranth, A.; Jayarambabu, N.; kumar, A.; Venkatappa Rao, T.; Kumar, R. R.; Srinivasa Rao, L. Novel Nanocomposite Polylactic Acid Films with Curcumin-ZnO: Structural, Thermal, Optical and Antibacterial Properties. *Current Res. Green Sustainable Chem.* **2022**, *5*, No. 100332.
(26) Misra, S. K.; Kondaiah, P.; Bhattacharya, S.; Rao, C. N. R. Graphene as a Nanocarrier for Tamoxifen Induces Apoptosis in Transformed Cancer Cell Lines of Different Origins. *Small* **2012**, *8* (1), 131−143.
(27) Ketabchi, M. R.; Khalid, M.; Ratnam, C. T.; Walvekar, R. Mechanical and Thermal Properties of Polylactic Acid Composites Reinforced with Cellulose Nanoparticles Extracted from Kenaf Fibre. *Mater. Res. Express* **2016**, *3* (12), No. 125301.
(28) Kim, Y.; Kim, J. S.; Lee, S.-Y.; Mahajan, R. L.; Kim, Y.-T. Exploration of Hybrid Nanocarbon Composite with Polylactic Acid for Packaging Applications. *Int. J. Biolog. Macromolecules* **2019**, *144*, 135 DOI: 10.1016/j.ijbiomac.2019.11.239.
(29) Poon, C. Y.; Bhushan, B. Comparison of Surface Roughness Measurements by Stylus Profiler, AFM and Non-Contact Optical Profiler. *Wear* **1995**, *190*, 76−88.
(30) Huhtamäki, T.; Tian, X.; Korhonen, J. T.; Ras, R. H. A. Surface-Wetting Characterization Using Contact-Angle Measurements. *Nat. Protoc* **2018**, *13* (7), 1521−1538.
(31) Shojaeiarani, J.; Bajwa, D. S.; Ryan, C.; Kane, S. Enhancing UV-Shielding and Mechanical Properties of Polylactic Acid Nanocomposites by Adding Lignin Coated Cellulose Nanocrystals. *Ind. Crops Prod* **2022**, *183*, No. 114904.
(32) Cardillo, D.; Sencadas, V.; Devers, T.; Monirul Islam, Md.; Tehei, M.; Rosenfeld, A.; Boutard, T.; Rocher, E.; Barker, P. J.; Konstantinov, K. Attenuation of UV Absorption by Poly(Lactic Acid)-Iron Oxide Nanocomposite Particles and Their Potential Application in Sunscreens. *Chem. Eng. J.* **2021**, *405*, No. 126843.
(33) Gandolfi, S.; Ottolina, G.; Riva, S.; Fantoni, G. P.; Patel, I. Complete Chemical Analysis of Carmagnola Hemp Hurds and Structural Features of Its Components *BioResources* 2013; Vol. *8* 2 DOI: 10.15376/biores.8.2.2641-2656.
(34) Mohammadi, M.; Bruel, C.; Heuzey, M. C.; Carreau, P. J. CNC Dispersion in PLA and PBAT Using Two Solvents: Morphological and Rheological Properties. *Cellulose* **2020**, *27* (17), 9877−9892.
(35) Zhu, H.; Wang, X.; Li, Y.; Wang, Z.; Yang, F.; Yang, X. Microwave Synthesis of Fluorescent Carbon Nanoparticles with Electrochemiluminescence Properties. *Chem. Commun.* **2009**, No. 34, 5118.
(36) Chandra, S.; Das, P.; Bag, S.; Laha, D.; Pramanik, P. Synthesis, Functionalization and Bioimaging Applications of Highly Fluorescent Carbon Nanoparticles. *Nanoscale* **2011**, *3* (4), 1533.
(37) Arrieta, M. P.; López, J.; López, D.; Kenny, J. M.; Peponi, L. Development of Flexible Materials Based on Plasticized Electrospun PLA-PHB Blends: Structural, Thermal, Mechanical and Disintegration Properties. *Eur. Polym. J.* **2015**, *73*, 433−446.
(38) Savenkova, L.; Gercberga, Z.; Nikolaeva, V.; Dzene, A.; Bibers, I.; Kalnin, M. Mechanical Properties and Biodegradation Characteristics of PHB-Based Films. *Process Biochem.* **2000**, *35* (6), 573−579.
(39) Sirasitthichoke, C.; Perivilli, S.; Liddell, M. R.; Armenante, P. M. Experimental Determination of the Velocity Distribution in USP Apparatus 1 (Basket Apparatus) Using Particle Image Velocimetry

(PIV). *Int. J. Pharm. X* **2021**, *3*, 1000078 DOI: 10.1016/j.ijpx.2021.100078.
(40) Hegyesi, N.; Zhang, Y.; Kohári, A.; Polyák, P.; Sui, X.; Pukánszky, B. Enzymatic Degradation of PLA/Cellulose Nanocrystal Composites. *Ind. Crops Prod.* **2019**, *141*, 111799 DOI: 10.1016/j.indcrop.2019.111799.
(41) Lee, S. H.; Kim, I. Y.; Song, W. S. Biodegradation of Polylactic Acid (PLA) Fibers Using Different Enzymes. *Macromol. Res.* **2014**, *22* (6), 657−663.
(42) Zimniewska, M. Hemp Fibre Properties and Processing Target Textile: A Review. *Materials* **2022**, *15* (5), 1901.
(43) Yang, G.; Park, S.-J. Conventional and Microwave Hydrothermal Synthesis and Application of Functional Materials: A Review. *Materials* **2019**, *12*, 1177 DOI: 10.3390/ma12071177.
(44) Bakshi, S.; He, Z.; Harris, W. G. A New Method for Separation, Characterization, and Quantification of Natural Nanoparticles from Soils. *J. Nanopart. Res.* **2014**, *16* (2), 2261 DOI: 10.1007/S11051-014-2261-1.
(45) Paramelle, D.; Sadovoy, A.; Gorelik, S.; Free, P.; Hobley, J.; Fernig, D. G. A Rapid Method to Estimate the Concentration of Citrate Capped Silver Nanoparticles from UV-Visible Light Spectra †. *The Analyst* **2014**, *139*, 4855−4861, DOI: 10.1039/c4an00978a.
(46) López-Rodríguez, A.; Mejía-Uriarte, E.; Sato-Berrú, R. A Practical Proposal for Silver Nanoparticles (Ag-NPs) Separation by Differential Centrifugation. *J. Nanopart. Res.* **2022**, *24* (12), 237 DOI: 10.1007/s11051-022-05609-x.
(47) Kister, G.; Cassanas, G.; Vert, M.; Pauvert, B.; Tbol, A. Vibrational Analysis of Poly(L-Lactic Acid). **1995**, *26*, 307. DOI: 10.1002/jrs.1250260409.
(48) Gan, L.; Geng, A.; Jin, L.; Zhong, Q.; Wang, L.; Xu, L.; Mei, C. Antibacterial Nanocomposite Based on Carbon Nanotubes-Silver Nanoparticles-Co-Doped Polylactic Acid. *Polymer Bulletin* **2020**, *77*, 793−804.
(49) Zambrzycki, M.; Sokolowski, K.; Gubernat, M.; Fraczek-Szczypta, A. Effect of Secondary Carbon Nanofillers on the Electrical, Thermal, and Mechanical Properties of Conductive Hybrid Composites Based on Epoxy Resin and Graphite. *Materials* **2021**, *14* (15), 4169 DOI: 10.3390/ma14154169.
(50) Xu, J.-Z.; Chen, T.; Yang, C.-L.; Li, Z.-M.; Mao, Y.-M.; Zeng, B.-Q.; Hsiao, B. S. Isothermal Crystallization of Poly(L-Lactide) Induced by Graphene Nanosheets and Carbon Nanotubes: A Comparative Study. *Macromolecules* **2010**, *43*, 5000−5008.
(51) Kim, Y.; Kim, J. S.; Lee, S. Y.; Mahajan, R. L.; Kim, Y. T. Exploration of Hybrid Nanocarbon Composite with Polylactic Acid for Packaging Applications. *Int. J. Biol. Macromol.* **2020**, *144*, 135−142.
(52) Du, J.; Cheng, H. M. The Fabrication, Properties, and Uses of Graphene/Polymer Composites. *Macromol. Chem. Phys.* **2012**, *213* (10−11), 1060−1077.
(53) Valapa, R. B.; Pugazhenthi, G.; Katiyar, V. Effect of Graphene Content on the Properties of Poly(Lactic Acid) Nanocomposites. *RSC Adv.* **2015**, *5*, 28410−28423, DOI: 10.1039/c4ra15669b.
(54) Valapa, R. B.; Pugazhenthi, G.; Katiyar, V. Effect of Graphene Content on the Properties of Poly(Lactic Acid) Nanocomposites. *RSC Adv.* **2015**, *5* (36), 28410−28423.
(55) Huang, H.-D.; Ren, P.-G.; Xu, J.-Z.; Xu, L.; Zhong, G.-J.; Hsiao, B. S.; Li, Z.-M. Improved Barrier Properties of Poly(Lactic Acid) with Randomly Dispersed Graphene Oxide Nanosheets. *J. Membr. Sci.* **2014**, *464*, 110−118.
(56) Lankone, R. S.; Wang, J.; Ranville, J. F.; Fairbrother, D. H. Photodegradation of Polymer-CNT Nanocomposites: Effect of CNT Loading and CNT Release Characteristics. *Environ. Sci. Nano* **2017**, *4* (4), 967−982.
(57) Borkotoky, S. S.; Dhar, P.; Katiyar, V. Biodegradable Poly (Lactic Acid)/Cellulose Nanocrystals (CNCs) Composite Microcellular Foam: Effect of Nanofillers on Foam Cellular Morphology, Thermal and Wettability Behavior. *Int. J. Biol. Macromol.* **2018**, *106*, 433−446.
(58) Alam, F.; Shukla, V. R.; Varadarajan, K. M.; Kumar, S. Microarchitected 3D Printed Polylactic Acid (PLA) Nanocomposite Scaffolds for Biomedical Applications. *J. Mech. Behav. Biomed. Mater.* **2020**, *103*, No. 103576.
(59) Mohd Nizar, M.; Hamzah, M. S. A.; Abd Razak, S. I.; Mat Nayan, N. H. Thermal Stability and Surface Wettability Studies of Polylactic Acid/Halloysite Nanotube Nanocomposite Scaffold for Tissue Engineering Studies, *In IOP Conference Series: Materials Science and Engineering*, Institute of Physics Publishing, 2018, Vol. 318.
(60) Das, K.; Ray, D.; Banerjee, I.; Bandyopadhyay, N. R.; Sengupta, S.; Mohanty, A. K.; Misra, M. Crystalline Morphology of PLA/Clay Nanocomposite Films and Its Correlation with Other Properties. *J. Appl. Polym. Sci.* **2010**, *118* (1), 143−151.
(61) Pinto, V. C.; Ramos, T.; Alves, A. S. F.; Xavier, J.; Tavares, P. J.; Moreira, P. M. G. P.; Guedes, R. M. Dispersion and Failure Analysis of PLA, PLA/GNP and PLA/CNT-COOH Biodegradable Nanocomposites by SEM and DIC Inspection. *Eng. Fail Anal.* **2017**, *71*, 63−71.
(62) Gallardo-Moreno, A. M.; Luque-Agudo, V.; González-Martín, M. L.; Hierro-Oliva, M. Micro-Structured and Self-Assembled Patterns in PLA-Cast Films as a Function of CTAB Content, Magnesium and Substratum Hydrophobicity. *Appl. Surf. Sci.* **2022**, *597*, No. 153676.
(63) Thakur, G.; Singh, A.; Singh, I. Formulation and Evaluation of Transdermal Composite Films of Chitosan-Montmorillonite for the Delivery of Curcumin. *Int. J. Pharm. Investig* **2016**, *6* (1), 23.
(64) Tyagi, P.; Gutierrez, J. N.; Lucia, L. A.; Hubbe, M. A.; Pal, L. Evidence for Antimicrobial Activity in Hemp Hurds and Lignin-Containing Nanofibrillated Cellulose Materials. *Cellulose* **2022**, *29* (9), 5151−5162.
(65) Khan, B. A.; Wang, J.; Warner, P.; Wang, H. Antibacterial Properties of Hemp Hurd Powder against < scp> E < /Scp>. Coli *J. Appl. Polym. Sci.* 2015, *13*210 DOI: 10.1002/app.41588.
(66) Cassano, R.; Trombino, S.; Ferrarelli, T.; Nicoletta, F. P.; Mauro, M. V.; Giraldi, C.; Picci, N. Hemp Fiber (Cannabis Sativa L.) Derivatives with Antibacterial and Chelating Properties. *Cellulose* **2013**, *20* (1), 547−557.
(67) Khan, B. A.; Warner, P.; Wang, H. Antibacterial Properties of Hemp and Other Natural Fibre Plants: A Review. *BioResources* **2014**, *9* (2), 3642−3659.
(68) Zampara, A.; Sørensen, M. C. H.; Grimon, D.; Antenucci, F.; Vitt, A. R.; Bortolaia, V.; Briers, Y.; Brøndsted, L. Exploiting Phage Receptor Binding Proteins to Enable Endolysins to Kill Gram-Negative Bacteria. *Sci. Rep.* **2020**, *10* (1), No. 12087.
(69) Singh, J.; Hegde, P. B.; Avasthi, S.; Sen, P. Scalable Hybrid Antibacterial Surfaces: TiO 2 Nanoparticles with Black Silicon. *ACS Omega* **2022**, *7*, 7816−7824, DOI: 10.1021/acsomega.1c06706.
(70) Chatterjee, A.; Perevedentseva, E.; Jani, M.; Cheng, C.-Y.; Ye, Y.-S.; Chung, P.-H.; Cheng, C.-L. Antibacterial Effect of Ultrafine Nanodiamond against Gram-Negative Bacteria *Escherichia Coli*. *J. Biomed Opt* **2015**, *20* (5), No. 051014.
(71) Shimpi, N.; Borane, M.; Mishra, S.; Kadam, M. Biodegradation of Polystyrene (PS)-Poly(Lactic Acid) (PLA) Nanocomposites Using Pseudomonas Aeruginosa. *Macromol. Res.* **2012**, *20* (2), 181−187.
(72) Kvien, I.; Tanem, B. S.; Oksman, K. Characterization of Cellulose Whiskers and Their Nanocomposites by Atomic Force and Electron Microscopy. *Biomacromolecules* **2005**, *6* (6), 3160−3165.
(73) Casas-Flores, S.; Domínguez-Espíndola, R. B.; Camposeco-solis, R.; Patrón-Soberano, O. A.; Rodríguez-González, V. Unraveling the Photoactive Annihilation Mechanism of Nanostructures as Effective Green Tools for Inhibiting the Proliferation of the Phytopathogenic Bacterium *Pseudomonas Syringae*. *Nanoscale Adv.* **2019**, *1* (6), 2258−2267.
(74) Zhong, C.; Saito, K.; Kawaguchi, K.; Setoue, H. The Hybrid Drop Test. *Packaging Technol. Sci.* **2014**, *27* (7), 509−520.
(75) Farris, A.; Pan, J.; Liddicoat, A.; Toleno, B. J.; Maslyk, D.; Shangguan, D.; Bath, J.; Willie, D.; Geiger, D. A.Drop Test Reliability of Lead-Free Chip Scale Packages. In *2008 58th Electronic Components and Technology Conference* 2008; pp 1173−1180.


https://doi.org/10.1021/acsomega.4c05732
*ACS Omega* 2024, 9, 45104−45116